ACCSCIENCE PUBLISHING

International Journal of Bioprinting

RESEARCH ARTICLE

Psoralen immunomodulation: *In vitro* macrophage reprogramming to enhance osseointegration of 3D-printed porous titanium scaffolds in osteoporosis

Jian Ji[1†], Jijie Peng[2,3†], Yilong Wu[4†], Yue Meng[5], Di Che[6], Siyan Chen[6], Jingyang Chen[6], Xingmao Zhou[6], Junzhe Wu[6*], Yufeng He[2,3*], and Yuzhu Wang[6*]

[1]Department of Breast Surgery, The Fifth Affiliated Hospital, Southern Medical University, Guangzhou, Guangdong, China

[2]State Key Laboratory of Mechanism and Quality of Chinese Medicine, Faculty of Chinese Medicine, Macau University of Science and Technology, Macao, Macao SAR, China

[3]Department of Traditional Treatment Center, Zhongshan Hospital of Traditional Chinese Medicine Affiliated to Guangzhou University of Traditional Chinese Medicine, Zhongshan, Guangdong, China

[4]Department of Orthopaedic Surgery, Faculty of Medicine, University of Miyazaki, Miyazaki, Miyazaki, Japan

[5]Department of Orthopaedic Surgery, The Fifth Affiliated Hospital, Southern Medical University, Guangzhou, Guangdong, China

[6]Department of Orthopaedic Surgery, Zhongshan Hospital of Traditional Chinese Medicine Affiliated to Guangzhou University of Traditional Chinese Medicine, Zhongshan, Guangdong, China

[†]These authors contributed equally to this work.

***Corresponding authors:**
Junzhe Wu (wujunzhe@zsszyy.net)

Yufeng He (heyufeng@zsszyy.net)

Yuzhu Wang (wangyuzhu@zsszyy.net)

Citation: Ji J, Peng J, Wu Y, *et al.* Psoralen immunomodulation: *In vitro* macrophage reprogramming to enhance osseointegration of 3D-printed porous titanium scaffolds in osteoporosis *Int J Bioprint*. 2026;12(1):540-558. doi: 10.36922/IJB025480495

Received: November 25, 2025
1st revised: December 15, 2025
2nd revised: December 22, 2025
Accepted: December 24, 2025
Published online: January 8, 2026

Abstract

Psoralen inhibits osteoclast activity and bone resorption while enhancing osteoblast activity and bone formation. However, its role in modulating macrophage polarization to enhance osteoblast function and scaffold osseointegration under osteoporotic conditions remains underexplored. We fabricated Voronoi-structured metal scaffolds by 3D printing and evaluated psoralen *in vitro* in a macrophage–bone marrow mesenchymal stem cell co-culture system using serum from psoralen-treated rats, and *in vivo* in an osteoporotic bone-defect model with oral psoralen administration. The results demonstrated that psoralen treatment promoted M2 macrophage polarization, increased the M2/M1 ratio, and upregulated osteogenic gene expression *in vitro*. Improved bone formation parameters—including bone volume fraction, trabecular thickness, and trabecular number—around the implanted scaffolds were observed *in vivo*. The findings suggest a synergistic effect between gradient scaffold structures and psoralen in enhancing M2-mediated osteogenesis. Taken together, these findings may provide novel strategies for improving bone repair and prosthesis integration in osteoporosis.

Keywords: Macrophage polarization; Osseointegration; Osteoporosis; Psoralen

1. Introduction

In osteoporosis, bone remodeling homeostasis is disrupted, and bone resorption exceeds bone formation.[1] Psoralen may help restore bone remodeling balance through bidirectional regulation: on the one hand, it promotes bone formation; on the other hand, it inhibits bone resorption.[2] Psoralen can promote the osteogenic differentiation of bone marrow mesenchymal cells.[3] It initiates and accelerates the formation of new bone by activating key osteogenic signaling pathways such as Wnt/β-catenin and upregulating the expression of key transcription factors such as Runx2 (the main regulatory factor of osteoblast differentiation) and Osterix.[4] In terms of bone resorption inhibition, psoralen mainly exerts its effect by interfering with the canonical pathway of receptor activator of nuclear factor-κB ligand/receptor activator of nuclear factor-κB/nuclear factor-κB (NF-κB). This pathway is the central signaling axis in the generation and activation of osteoclasts. By inhibiting this pathway, psoralen can effectively reduce the formation of osteoclasts and lower their bone resorption activity.[5]

Psoralen may promote tissue repair by modulating macrophage polarization. Psoralen has been reported to inhibit nitric oxide (NO) production and 15-lipoxygenase activity and reduced pro-inflammatory Th1 cytokines (e.g., interferon [IFN]-γ, tumor necrosis factor [TNF]-α, and interleukin [IL]-2) while increasing the secretion of anti-inflammatory cytokines (e.g., IL-4, IL-6, and IL-10) in activated RAW 264.7 macrophage cells.[6] Further studies showed that psoralen inhibited the phosphorylation of Fyn and protein kinase Cδ, thereby inhibiting the activation of the mitogen-activated protein kinase and NF-κB pathways and suppressing the expression of pro-inflammatory cytokines in microglia.

Furthermore, psoralen reduced oxidative stress, neuronal damage, and apoptosis by inhibiting neuroinflammation. It decreased the expression of inducible NO synthase, cluster of differentiation (CD)-86, and TNF-α, and increased the expression of arginase-1, CD206, and IL-10. This indicates that psoralen inhibited the M1 microglial phenotype and promoted the M2 microglial phenotype.[7] However, osseointegration of titanium alloy scaffolds is often compromised in osteoporosis because of a dysregulated inflammatory microenvironment. Few studies have investigated whether psoralen can enhance titanium scaffold bone ingrowth by modulating macrophage polarization.

This study examined whether psoralen promotes osseointegration in osteoporotic bone defects by modulating macrophage polarization. We designed Voronoi-based scaffolds by metal three-dimensional (3D) printing, evaluated osteogenesis in a scaffold–macrophage–bone marrow-derived mesenchymal stem cell (BMSC) co-culture system, and validated scaffold osseointegration in an ovariectomy (OVX)-induced osteoporotic rat model.

2. Materials and methods

2.1. Design of the porous scaffolds

Using a multi-modal approach (Figure 1A), we systematically assessed how psoralen affects the immuno-osteogenic properties of Voronoi-based scaffolds. These scaffolds feature irregular pores created computationally using Voronoi tessellation theory. Each Voronoi cell follows the geometric principle described in **Equation (1)**, where points inside it are closer to its own seed point than to any other seed.[8] We designed two types of these Voronoi structures, namely, uniform irregular (UI; Figure S1) and graded irregular (GI; Figure S2), using Rhino 7's Grasshopper interface (McNeel & Associates, USA). By controlling seed distribution and strut thickness (Figure 1B and C; Table 1), the GI and UI structures were designded.[9]

$$V(P_i) = \{P/d(P, P_i) \leq d(P, P_j), j \neq i, j = 1, \ldots \ldots, n\} \quad (1)$$

where:

P_i is the core seed point of a sub-region space;

P is any point within the sub-region space other than P_i;

P_j is the core seed point in another sub-region space;

d is the distance between two points;

V represents the sub-region space.

This platform uses advanced algorithms to precisely control key design features, including seed density (N) and strut thickness. These parameters directly affect the scaffold's effective elastic modulus and porosity (P). The relationship between porosity and seed count is given by the following equations:

$$P = \frac{V_{total} - V_s}{V_{total}} \times 100\% \quad (2)$$

$$N \approx \frac{V_{total} \times P_1}{\frac{4 \times \pi}{3} \times r_1^3} \quad (3)$$

where V_{total} is the volume of the specific design space, V_s is the solid volume of the structure, P is the porosity of the porous structure, P_1 is the target porosity, r_1 is the target

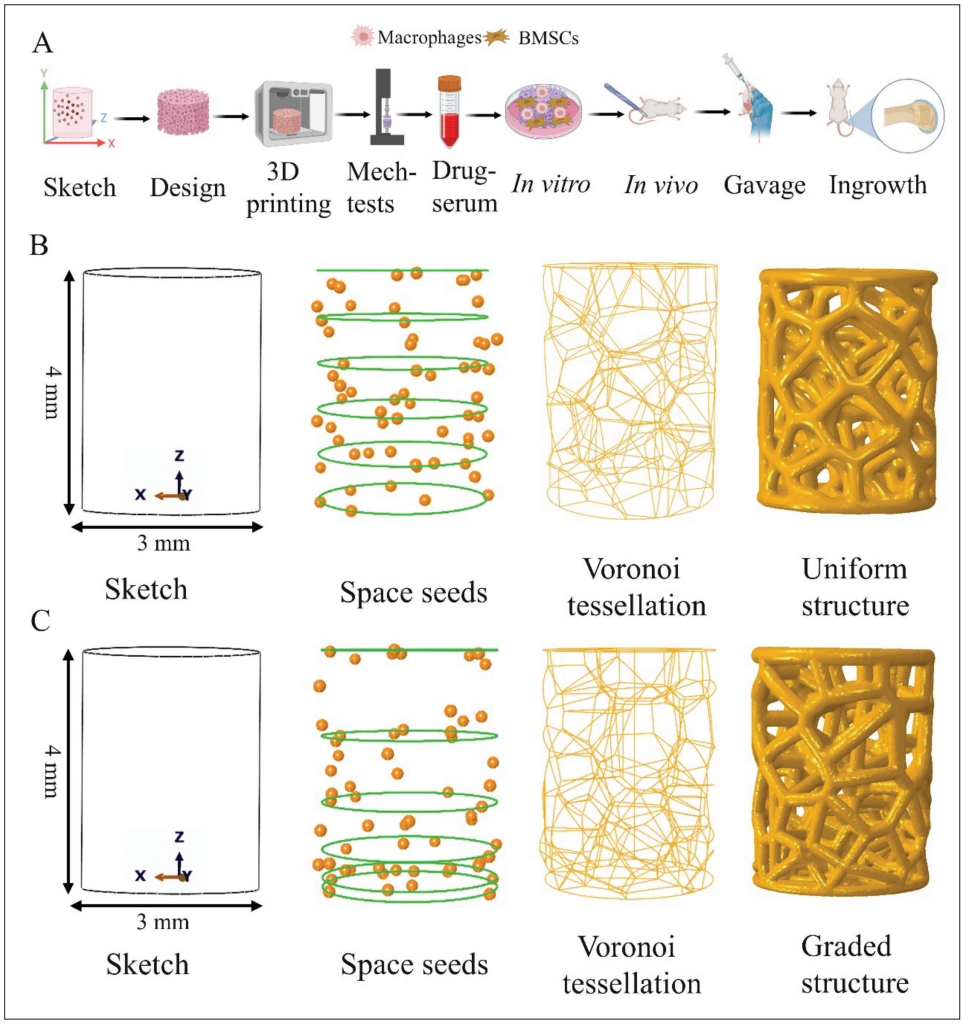

Figure 1. Bio-psoralen intervention for osteoporotic scaffold osseointegration: (A) Schematic illustration of bio-psoralen intervention on scaffold osseointegration under osteoporotic conditions, (B) design of the uniform scaffold, and (C) design of the graded scaffold. Abbreviations: 3D, three-dimensional; BMSC, bone marrow-derived mesenchymal stem cell.

Table 1. Construction of Voronoi-based scaffolds

Porosity (%)	UI structure[a]			GI structure[a]		
	Seeds (*N*)	Scale factors	Effective Volumes (mm^3)	Seeds (*N*)	Scale factors	Effective Volumes (mm^3)
44	60	0.17	15.57	60	0.09–0.234	15.57
52		0.155	13.46		0.09–0.208	13.46
59		0.141	11.41		0.09–0.182	11.41
66		0.126	9.44		0.09–0.155	9.44
73		0.112	7.61		0.09–0.129	7.61

Note:[a]The volumes of bulk Ti-64 alloy are 28.26 mm^3 (3(Ø) × 4(h) mm^3). Abbreviations: GI: graded irregular; UI: uniform irregular.

average pore radius of the structure, and N is the number of seeds.

2.2. Three-dimensional printing of the metal scaffolds

The computer-aided design models were fabricated via selective laser sintering (Farsoon FS273M, Farsoon Technologies, China) using Ti6Al4V powder under specified conditions (Table 2). A total of 12 scaffolds ($n = 6$ per group) were printed at 59% porosity (reported to promote bone ingrowth when exceeding 50%) for both UI and GI types (Figure 2A).

After printing, scaffolds were removed, and the surfaces were polished using zirconia sandblasting. They were then ultrasonically cleaned sequentially in acetone, anhydrous ethanol, and deionized water (15 min each), followed by disinfection and high-temperature drying.[10]

Scaffold architecture was verified using micro-computed tomography (micro-CT) (Bruker SkyScan1276, Bruker, USA) with DataViewer (Bruker, USA) and CTvox software (Bruker, USA) (Figure 2B). SEM imaging revealed smooth surfaces on both UI (Figure 2C) and GI (Figure 2D) scaffolds, with no significant cracks or powder residue.[11]

2.3. Experimental mechanical tests of the scaffolds

We tested UI and GI scaffolds (Figure 2E) under quasi-static compression along the z-axis with a QX-W600 universal testing machine (Qixiang Corp., China). The stiffness was calculated from the stress–strain curves using **Equation (4)**:

$$E_{effective} = \frac{\sigma}{\varepsilon} = \frac{F_R / A}{\Delta h / h} \quad (4)$$

where F_R, A, Δh, and h represent the reaction force, cross-sectional area, change in length, and original length of the porous structure, respectively. The GI scaffolds showed a significantly lower effective elastic modulus (1539.5 ± 180.01 MPa) than the UI structures (2163.3 ± 138.42 MPa), as observed in the stress–strain curves (Figure 2F) and modulus comparison (Figure 2G).[12]

2.4. Immuno-osteogenic differentiation testing *in vitro*

2.4.1. Preparation of osteoporosis and bio-psoralen containing serum

The study protocol was approved by the Ethics Committee of Zhongshan Hospital of Traditional Chinese Medicine, Guangzhou University of Chinese Medicine (AEWC-2023008; SYXK 2020–0109). Figure 3A illustrates the intervention of bio-psoralen on scaffold-mediated macrophage regulation under osteoporotic conditions *in vitro* and its effects on bone ingrowth *in vivo*.

A total of 30 female 2-month-old Sprague–Dawley rats—obtained from the Guangdong Medical Animal Laboratory Center (approval no.: SCXK 2022-0002)—were randomly divided into three groups: normal (N; $n = 10$), OVX-induced osteoporosis (OP; $n = 10$), and OVX + bio-psoralen (BP; $n = 10$) groups.

All rats were housed under specific pathogen-free conditions with *ad libitum* access to food. After 2 weeks of acclimation, OP and BP groups underwent bilateral OVX under isoflurane anesthesia (3% induction, 2% maintenance; 1.2 L/min O_2), while the N group received sham surgery (skin incision only).

To confirm successful model establishment, one randomly selected surviving rat from the N group and one from the OP group were subjected to dual-energy X-ray absorptiometry of the lumbar vertebrae after 10 weeks of observation.

Following confirmation of osteoporosis induction in the OP and BP groups, bio-psoralen (Jule Pharmaceutical Co., China) was administered orally to the BP group at a dose of 14 mg/kg/day, dissolved in 0.9% sodium chloride solution. After 4 weeks, all rats were anesthetized, and blood was collected via abdominal aorta puncture. The samples were centrifuged, and the serum was stored at −80°C for subsequent *in vitro* experiments.[13]

Table 2. Parameter settings of three-dimensional metal printing by selective laser sintering

Materials	Technical type	Layer thickness (mm; range)	Fill laser power (W; range)	Fill speed (mm/s; range)	Support laser power (W; range)	Support speed (mm/s; range)	Hatch spacing (mm; range)	Atmosphere (O_2 level) (%)	Powder specs (mm)	Build orientation
Ti-6Al-4V	Selective laser sintering	0.035 (0.03–0.04)	200 (150–250)	1,000 (950–1,250)	100 (50–170)	500 (400–700)	0.1 (0.08–0.12)	0.06	$D_{10} = 0.02$, $D_{50} = 0.034$	90° (z-axis)

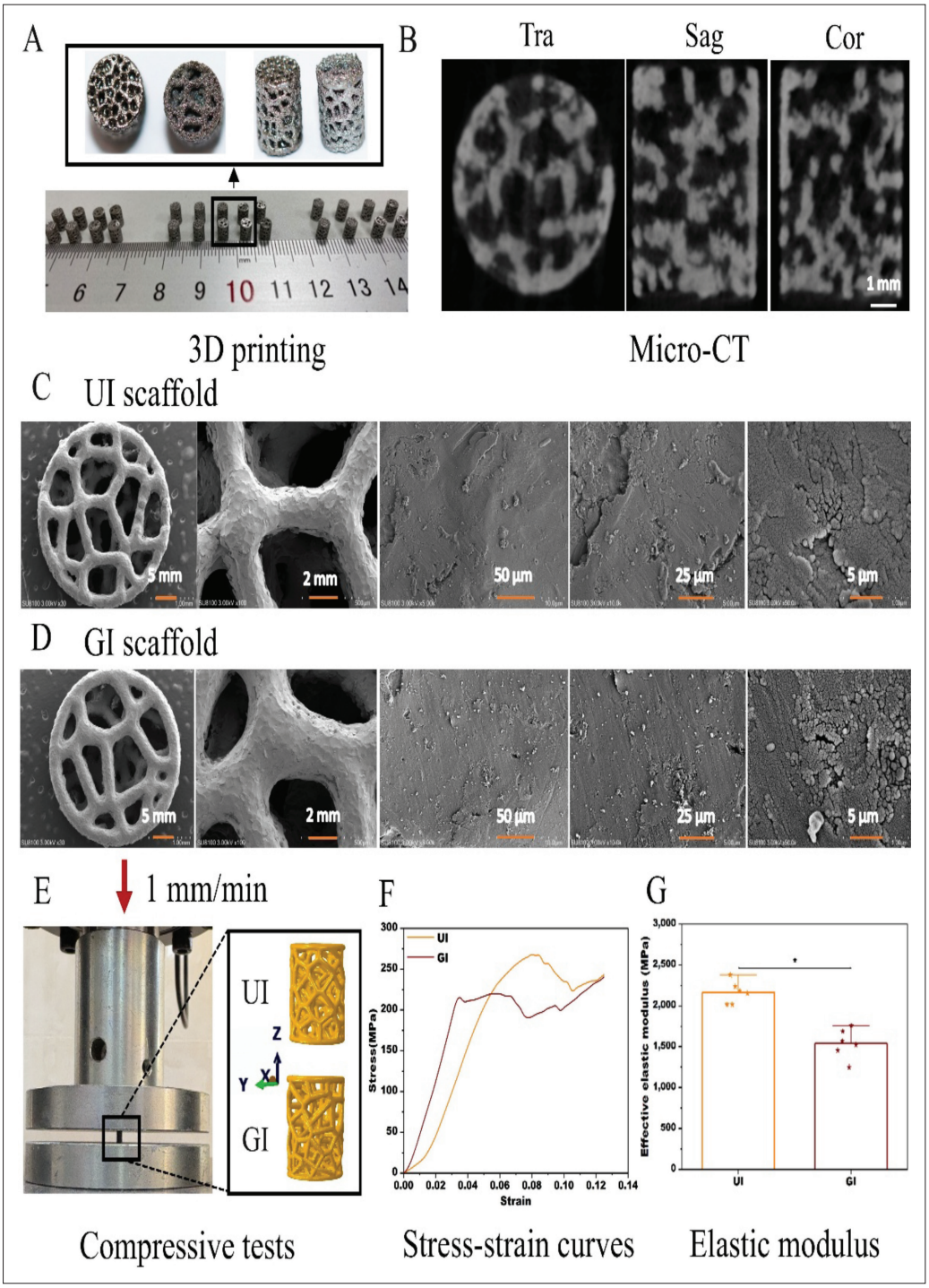

Figure 2. Biomechanical properties and 3D printing of porous metal scaffolds: (A) 3D printing of the porous metal scaffolds, (B) micro-CT images of the porous specimens (scale bar: 1 mm; magnification: 50×), (C) surface morphology of uniform scaffolds observed using scanning electron microscope (scale bar: 5 mm, magnification: 10×; scale bar: 2 mm, magnification: 20×; scale bar: 50 μM, magnification: 100×; scale bar: 25 μM, magnification: 200×; scale bar: 5 μM, magnification: 1000×), (D) surface morphology of the graded scaffolds observed using scanning electron microscope (scale bar: 5 mm, magnification: 10×; scale bar: 2 mm, magnification: 20×; scale bar: 50 μM, magnification: 100×; scale bar: 25 μM, magnification: 200×; scale bar: 5 μM, magnification: 1000×), (E) mechanical testing of the porous scaffolds, (F) representative stress–strain curves of the scaffolds, and (G) effective elastic modulus of the scaffolds ($n = 6$). Data are expressed as the mean ± standard deviation. $^{*}p < 0.05$ and $^{**}p < 0.01$ indicate statistical significance. Abbreviations: 3D: three-dimensional; Cor: coronal section; CT: computed tomography; GI: graded irregular; UI: uniform irregular; Sag: sagittal section; Tra: transverse section.

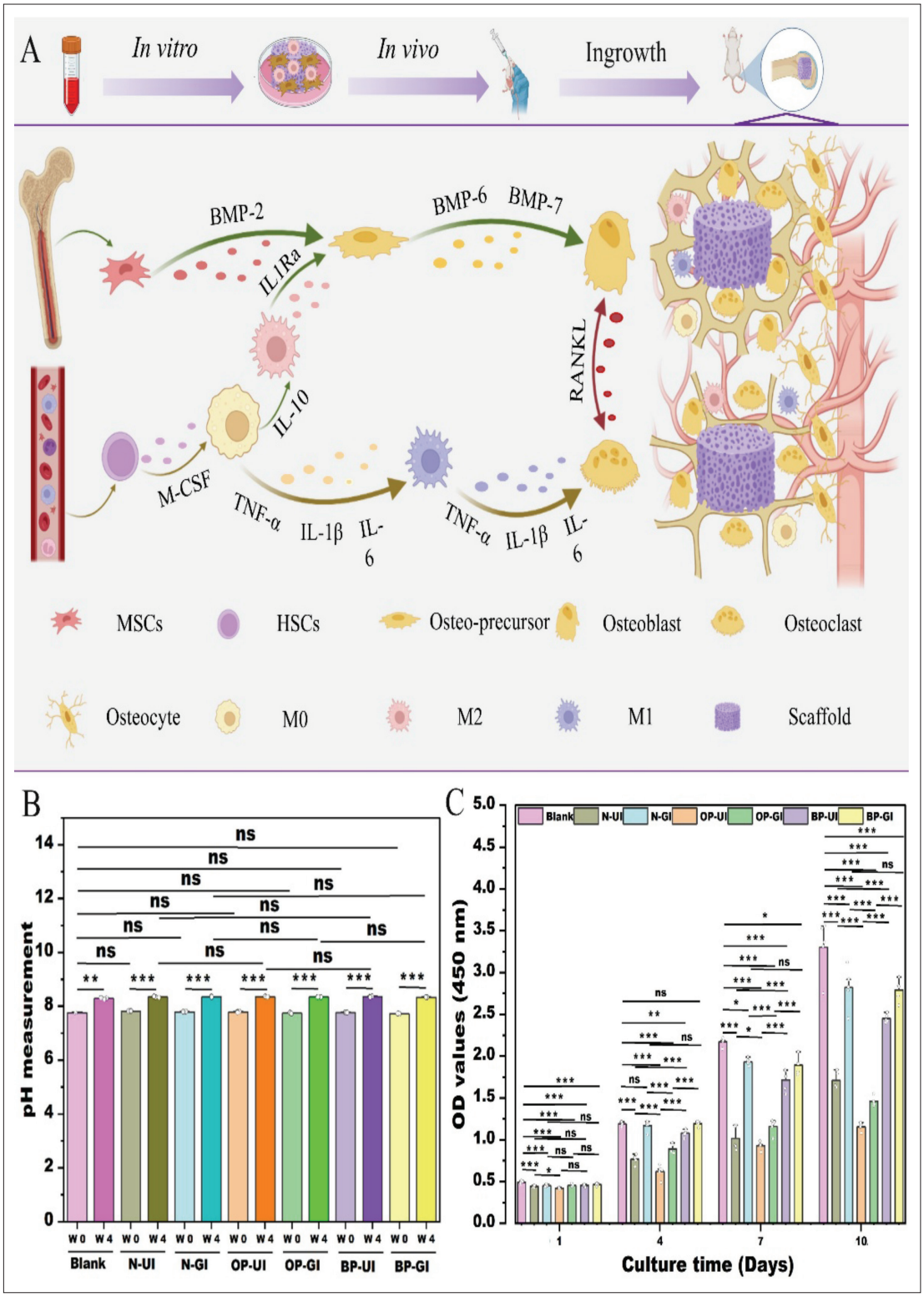

Figure 3. Effect of BP on cell proliferation. (A) Schematic illustration of macrophage polarization-mediated bone remodeling around implants regulated by BP; (B) pH measurement of scaffold-conditioned culture media at different time points (n = 3); and (C) cell proliferation assessed at different time points (n = 5). Data are expressed as mean ± standard deviation. $^{*}p < 0.05$, $^{**}p < 0.01$, and $^{***}p < 0.001$ indicate statistical significance. Abbreviations: ns: no statistical significance; BP: bio-psoralen; GI: graded irregular; HSC: hematopoietic stem cell; MSC: mesenchymal stem cell; N: normal; OD: optical density; OP: osteoporosis; UI: uniform irregular.

2.4.2. Preparation of scaffold-conditioned medium

After ultrasonic cleaning in acetone, ethanol, and deionized water (15 min each), scaffolds were air-dried and autoclaved. UI and GI scaffolds were then immersed for 4 weeks in three types of serum: the N, OP, and BP group sera. For the blank control, scaffolds were incubated in α-Minimum Essential Medium supplemented with 10% fetal bovine serum (Gibco, USA), 100 μg/mL streptomycin (Gibco, USA), and 100 U/mL penicillin (Gibco, USA). The pH of the scaffold-conditioned media was measured before and after the 4 weeks of immersion in the serum (n = 3). Scaffold surfaces were examined post-immersion using high-resolution SEM to assess structural changes.

2.4.3. Culture of bone mesenchymal stem cells

Rat BMSCs (rBMSCs) were isolated from the femoral bone marrow of 4-week-old Sprague–Dawley rats (n = 10). Cells were cultured in α-Minimum Essential Medium at 37°C with 5% CO_2, passaged at a 1:3 ratio, and used at passage 3.

2.4.4. Culture of macrophage cells

The RAW264.7 murine macrophage cell line (Shanghai Institutes for Biological Sciences, China) was cultured in growth medium containing 10% fetal bovine serum, 100 U/mL penicillin, and 100 μg/mL streptomycin at 37°C with 5% CO_2. Cells were passaged at a 1:3 ratio and used between passages 3 and 5.

2.4.5. Cell proliferation testing

Rat BMSCs were seeded in 24-well plates and cultured in scaffold-conditioned medium. Cell proliferation was assessed at days 1, 4, 7, and 10 using the cell counting kit (CCK)-8 assay following the manufacturer's instructions, and the absorbance was measured at 450 nm (n = 3).

2.4.6. Macrophage phenotypic characterization

RAW264.7 macrophages were seeded in 12-well plates and stimulated with 100 ng/mL lipopolysaccharide (LPS) in serum-free medium for 6 h at approximately 80% confluency to model acute inflammation. Cells were then cultured in scaffold-conditioned medium for 3 days. Immunostaining was performed using fluorescein isothiocyanate-conjugated anti-CD11c (M1 macrophage marker; 1:400; 11-0114-82, Thermo Fisher Scientific, USA) and allophycocyanin-conjugated anti-CD206 (M2 macrophage marker; 1:300; 17-2061-82, Thermo Fisher Scientific, USA) in phosphate-buffered saline/1% bovine serum albumin for 1 h.

Flow cytometric analysis was conducted using a sequential gating strategy with debris and doublet exclusion, starting from the total cell population. Debris was excluded first, followed by sequential gating to identify the target macrophage subpopulations. Data were acquired using a CytoFLEX LX (Beckman Coulter, USA) and analyzed with CytExpert 2.4 software (Beckman Coulter, USA) using standardized gating parameters.

2.4.7. Detection of gene expression related to macrophage polarization and inflammation

RAW264.7 cells in 24-well plates underwent RNA extraction and reverse transcription to cDNA. Gene expression of TNF-α, IL-1β, IL-6, IL-1Ra, IL-10, and arginase-1 was analyzed by real-time quantitative polymerase chain reaction.

2.4.8. Preparation of scaffold-modulated macrophage conditioned media

To assess how scaffold-conditioned macrophage secretions affect rBMSC osteogenic differentiation, we collected conditioned medium from polarized RAW264.7 cells. Macrophages in T75 flasks (approximately 80% confluency) were primed with 100 ng/mL LPS for 6 h and then cultured in scaffold-conditioned serum medium. After incubation, the culture media were centrifuged, and the supernatants were mixed at a 1:2 ratio with fresh growth medium. Conditioned medium from macrophages cultured without scaffold exposure served as the control.

2.4.9. Alkaline phosphatase activity assay

Alkaline phosphatase (ALP) activity in rBMSCs was measured spectrophotometrically (405 nm) after 4 and 7 days using a commercial ALP activity kit (EEA002, Thermo Fisher Scientific, USA) to assess early osteogenic differentiation. Mineralization was evaluated at day 14 via alizarin red staining (quantified at 630 nm). Osteogenic gene expression (*Alp*, *Col1*, *Ocn*, *Runx2*, *Opn*) was analyzed using real-time quantitative reverse transcription polymerase chain reaction.

2.5. *In vivo* evaluation of scaffolds

2.5.1. Preparation of osteoporotic animals

A total of 72 female 2-month-old Sprague–Dawley rats—obtained from the Guangdong Medical Animal Laboratory Center—were randomly divided into three treatment groups: normal (N; sham surgery), OP (OVX-induced osteoporosis), and BP (OVX + bio-psoralen). Each treatment group was further subdivided according to scaffold type (UI or GI) and implantation time point, resulting in 12 experimental groups (n = 6 per group).

Samples were collected at 4 and 8 weeks to evaluate osseointegration, with six groups assessed at each time point (4 weeks: N-UI 4W, N-GI 4W, OP-UI 4W, OP-GI 4W, BP-UI 4W, and BP-GI 4W; 8 weeks: N-UI 8W, N-GI 8W, OP-UI 8W, OP-GI 8W, BP-UI 8W, and BP-GI 8W).

All rats were housed under specific pathogen-free conditions with *ad libitum* access to food. After 2 weeks of acclimation, the OP and BP groups underwent bilateral OVX under isoflurane anesthesia (3% induction, 2% maintenance), while the N group received sham surgery (skin incision only). To confirm successful osteoporosis induction, one randomly selected surviving rat from the N group and one from the OP group were subjected to dual-energy X-ray absorptiometry of the lumbar vertebrae after 10 weeks of observation.

2.5.2. Scaffold implantation and bio-psoralen intervention

Following confirmation of osteoporosis induction, the right femoral condyle of rats in the relevant groups received pre-sterilized UI or GI single scaffold (59% porosity) under isoflurane anesthesia.

After prone positioning and skin disinfection, a 3-cm longitudinal incision was made to expose the right femoral condyle. Scaffolds were implanted into drilled sites and irrigated with saline solution. After 1 week, ovariectomized rats received an oral bio-psoralen suspension, prepared by dissolving bio-psoralen in 0.9% sodium chloride solution, and administered via gavage at a dose of 14 mg/kg per day.

After 4 and 8 weeks of bio-psoralen intervention, rats were euthanized by cervical dislocation. The right femurs were dissected, soft tissue removed, fixed in 4% paraformaldehyde, and stored at 25°C for micro-CT analysis.

2.5.3. Micro-computed tomography images and analysis

Bone–scaffold complexes were scanned via micro-CT (SkyScan1276, Bruker) at 10 μm isotropic resolution (80 kV, 100 μA). Reconstructed images were analyzed using CTAn software (Bruker, USA) to quantify new bone parameters: bone volume fraction (BV/TV; %), trabecular thickness (Tb.Th; mm), and trabecular number (Tb.N; mm^{-1}).

2.5.4. Histological staining evaluation

New bone regeneration was assessed histologically. Bone–scaffold complexes were fixed in 10% formaldehyde for 7 days at 4°C, rinsed overnight, dehydrated through graded ethanol, cleared in xylene, and embedded in polymethyl methacrylate. Sections (800 μm thick) were cut perpendicular to the implant axis using a Leica 1600 microtome (Leica Microsystems, Germany), stained with Toluidine Blue and Van Gieson's (VG), and examined under a Leica DMLA microscope (Leica Microsystems, Germany) at 40× and 100× magnification.

2.6. Statistical analysis

Data were analyzed using SPSS 17.0 (IBM, USA) and visualized in Origin Pro 2021b (Northampton, USA). Group comparisons were conducted using one-way ANOVA with Tukey's post hoc correction. Results are presented as mean ± standard deviation. $^{*}p < 0.05$, $^{**}p < 0.01$, $^{***}p < 0.001$, and $^{****}p < 0.0001$ were considered statistically significant.

3. Results

3.1. Proliferation of bone mesenchymal stem cells in scaffold-conditioned media

The findings revealed that the pH of all scaffold-conditioned media increased after 4 weeks of immersion, with no significant differences between groups at the endpoint (Figure 3B), indicating minimal influence of scaffolds on medium chemistry. BMSC proliferation, assessed by the CCK-8 assay, increased over 10 days, with the BP group showing higher activity than the OP group but lower than the N group and blank controls (Figure 3C). SEM revealed no structural defects or degradation after 4 weeks of media immersion (Figure 4).

Live/dead staining showed decreasing BMSC viability in the OP-scaffold groups over 7 days, with dead cells visible at days 4 and 7. In contrast, N- and BP-scaffolds maintained high cellular viability throughout the observation period, showing no discernible signs of cell death (Figure 5). The proliferation trend indicated by CCK-8 correlated well with the cell viability patterns observed via live/dead staining.

3.2. Macrophage phenotype and marker expression in different culture media

Flow cytometry showed a higher M2/M1 ratio in BP-scaffolds than in OP-scaffolds, although both were lower than the N group. The N- and BP-scaffolds favored M2 polarization, whereas OP-scaffolds skewed toward M1 (Figure 6A).

Pro-inflammatory cytokines (e.g., TNF-α, IL-1β, and IL-6) were elevated in OP vs. BP scaffolds, and in UI vs. GI scaffolds (Figure 6B–D), while anti-inflammatory markers (IL-1Ra, IL-10, arginase-1) were higher in BP vs. OP scaffolds and in GI vs. UI scaffolds, but remained below normal levels (Figure 6E–G).

3.3. Osteogenic differentiation of bone mesenchymal stem cells in different culture media

Osteogenic induction assessed by alizarin red staining and ALP activity revealed that ALP activity and osteogenic nodule formation in BP-scaffold groups were higher than in OP groups, and in GI groups were higher than in UI groups (Figure 7A–C). RT-PCR analysis indicated that the gene expression of *Alp*, *Opn*, *Ocn*, *Col1*, and *Runx2* (week 4: Figure 7D–H; week 8: Figure 7I–M) in BP-scaffold

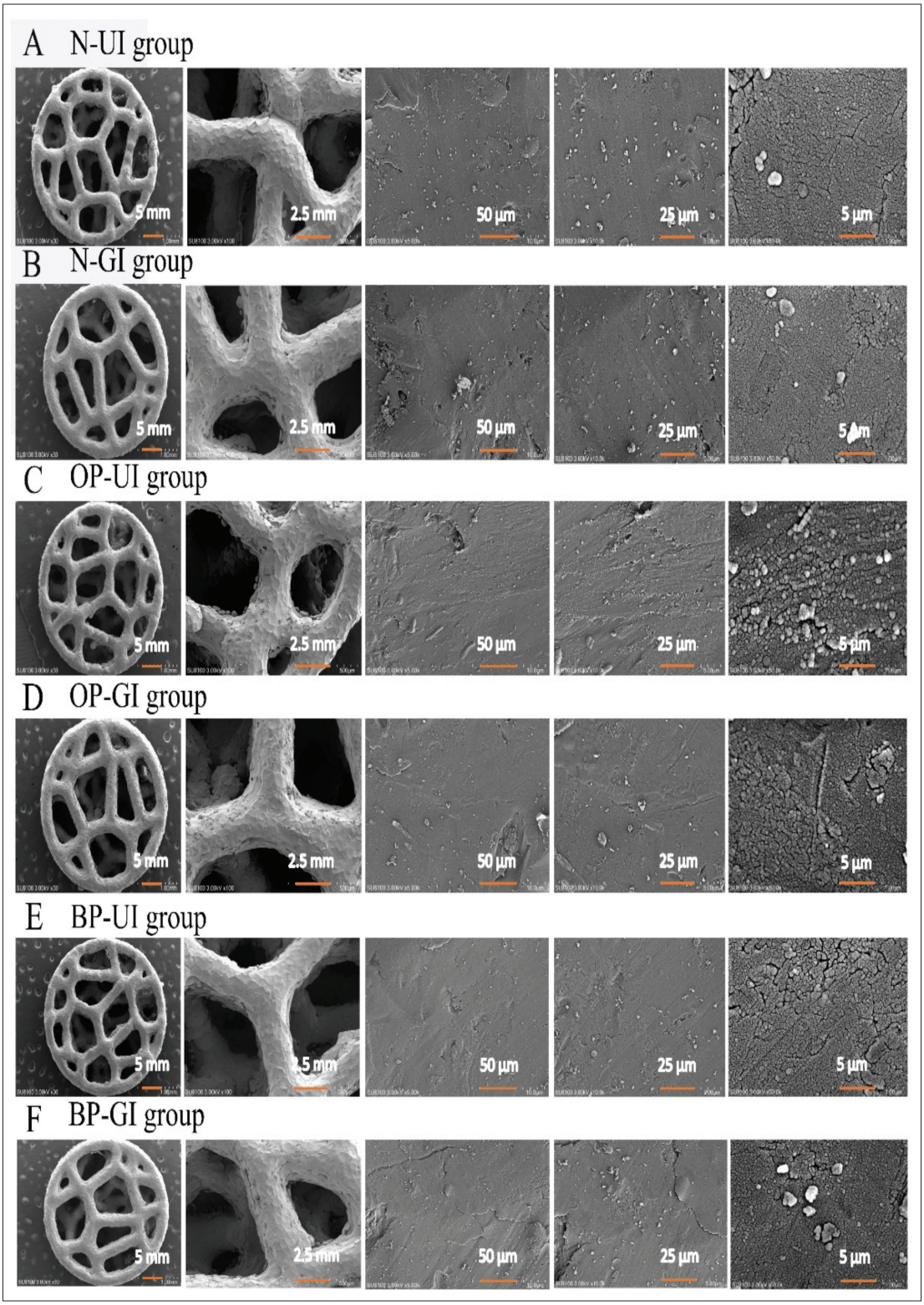

Figure 4. Surface morphology of the specimens after 4 weeks of immersion in different media: (A) N-UI, (B) N-GI, (C) OP-UI, (D) OP-GI, (E) BP-UI, and (F) BP-GI (scale bar: 5 mm, magnification: 10×; scale bar: 2.5 mm, magnification: 20×; scale bar: 50 μM, magnification: 100×; scale bar: 25 μM, magnification: 200×; scale bar: 5 μM, magnification: 1000×). Abbreviations: BP: bio-psoralen; GI: graded irregular; N: normal; OP: osteoporosis; UI: uniform irregular.

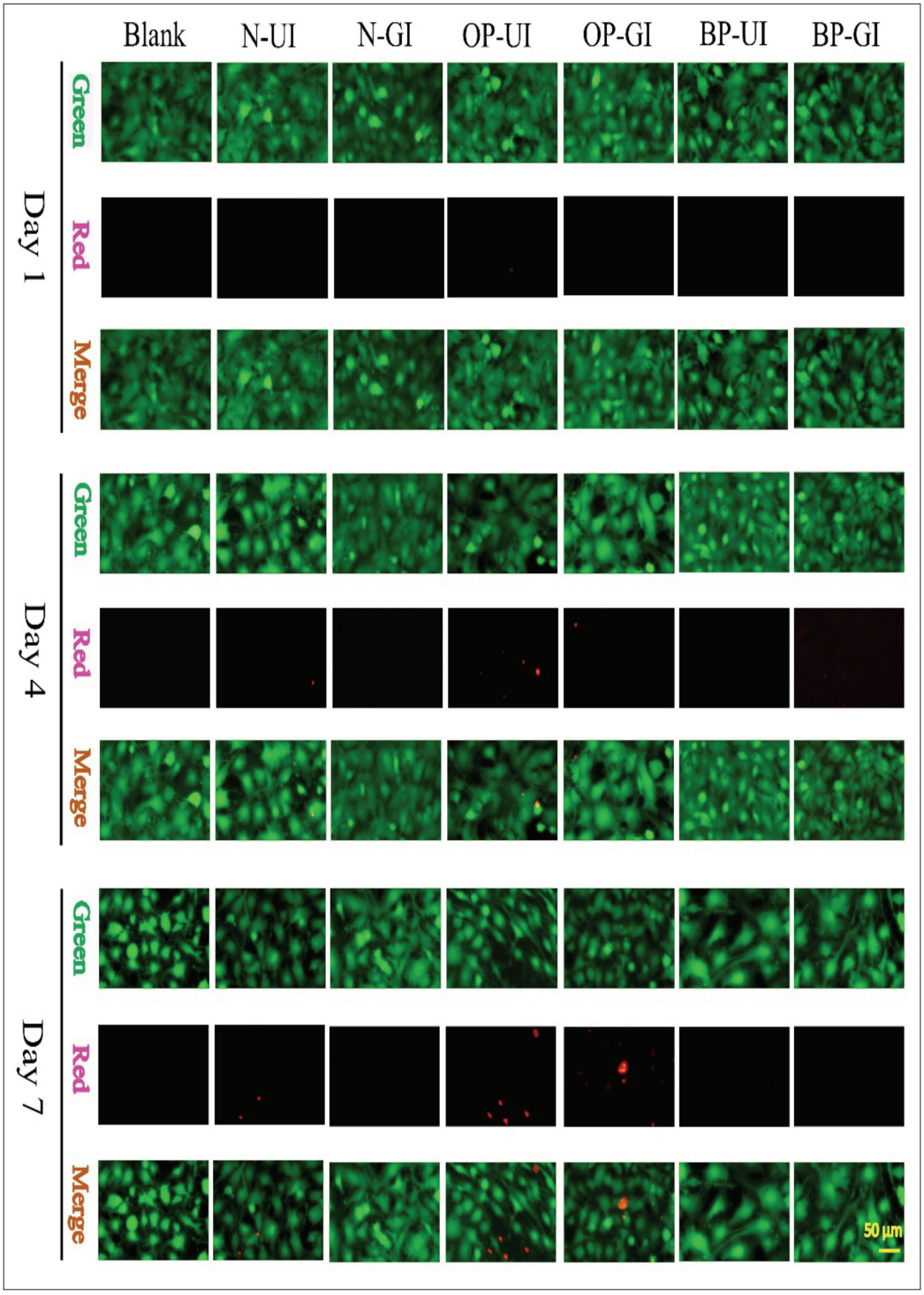

Figure 5. Cell morphology assessed using immunofluorescence double staining at different time points. Green indicates live cells, and red indicates dead cells (scale bar: 50 μm; magnification: 100×). Abbreviations: BP: bio-psoralen; GI: graded irregular; N: normal; OP: osteoporosis; UI: uniform irregular.

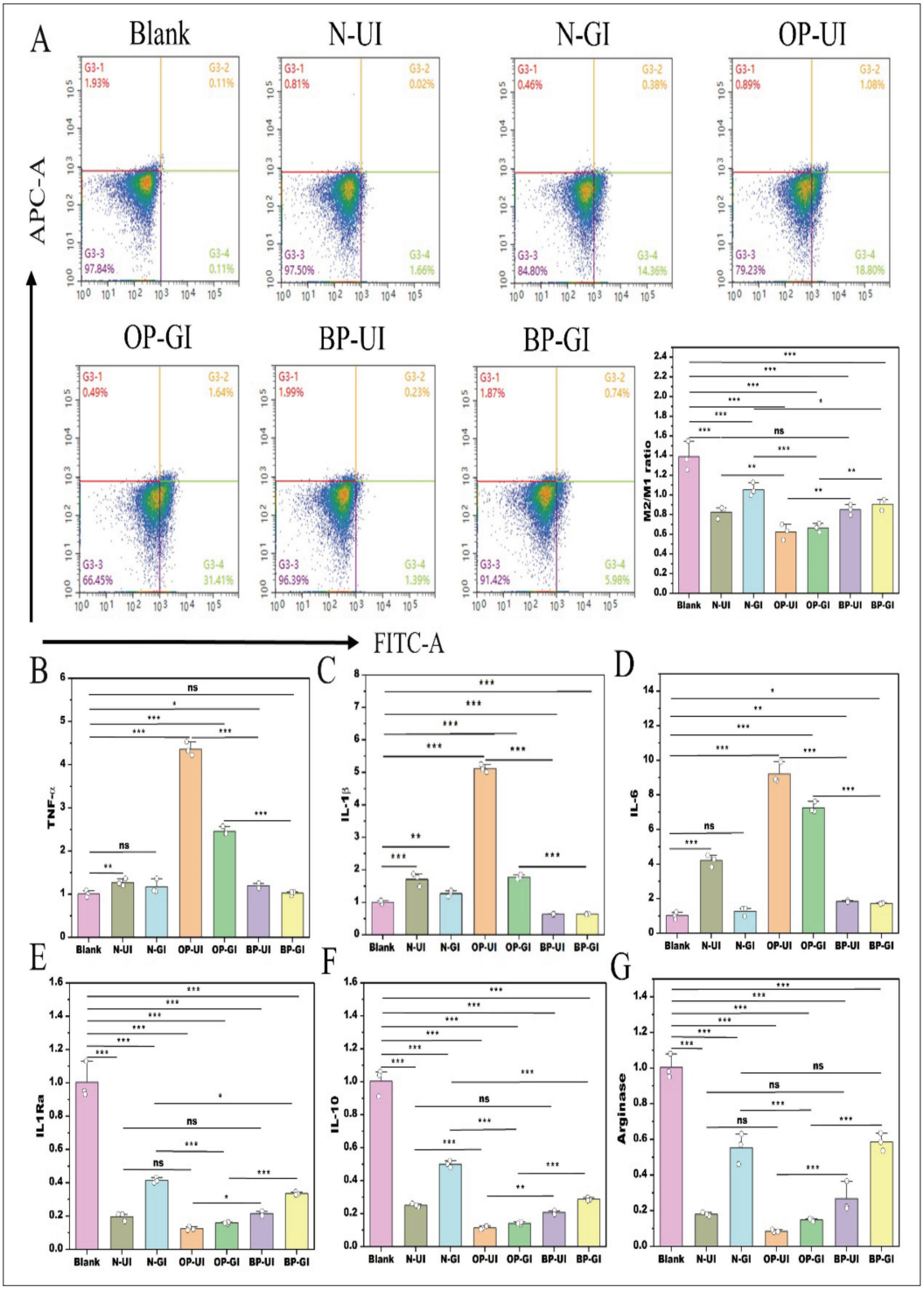

Figure 6. Macrophage expression in different culture media. (A) M2/M1 macrophage ratio determined by dual-labeling flow cytometry. (B–G) Expression of cytokines and markers: (B) TNF-α, (C) IL-1β, (D) IL-6, (E) IL-1Ra, (F) IL-10, and (G) arginase. Data are expressed as mean ± standard deviation ($n = 3$). $^{*}p < 0.05$, $^{**}p < 0.01$, $^{***}p < 0.001$, and $^{****}p < 0.0001$ indicate statistical significance. Abbreviations: ns: no statistical significance; APC: allophycocyanin; BP: bio-psoralen; FITC: fluorescein isothiocyanate; GI: graded irregular; IL: interleukin; N; normal; OP: osteoporosis; TNF: tumor necrosis factor; UI: uniform irregular.

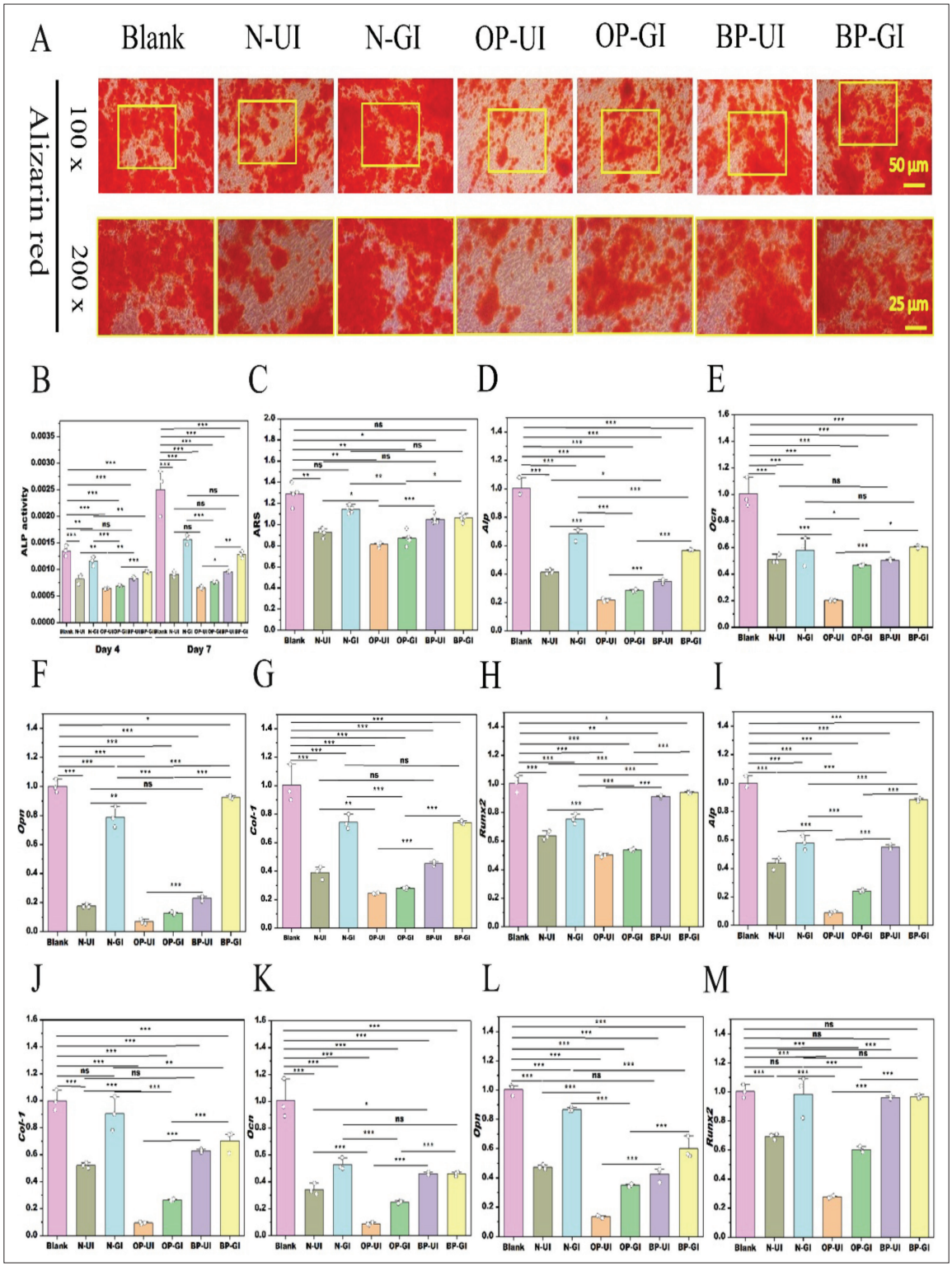

Figure 7. *In vitro* osteogenic differentiation of cells. (A) Extracellular matrix mineralization assessed by ARS (scale bar: 50 μm, magnification: 100×; scale bar: 25 μm, magnification: 200×). (B) ALP activity of cells at different time points ($n = 3$). (C) ARS quantification of extracellular matrix mineralization ($n = 5$). (D–H) Gene expression at week 4 ($n = 3$): (D) *Alp*, (E) *Ocn*, (F) *Opn*, (G) *Col1*, and (H) *Runx2*. (I–M) Gene expression at week 8 ($n = 3$): (I) *Alp*, (J) *Ocn*, (K) *Opn*, (L) *Col1*, and (M) *Runx2*. Data are expressed as the mean ± standard deviation. $^{*}p < 0.05$, $^{**}p < 0.01$, $^{***}p < 0.001$, and $^{****}p < 0.0001$ indicate statistical significance. Abbreviations: ns: no statistical significance; ALP: alkaline phosphatase; ARS: alizarin red staining; BP: bio-psoralen; GI: graded irregular; N: normal; OP: osteoporosis; UI: uniform irregular.

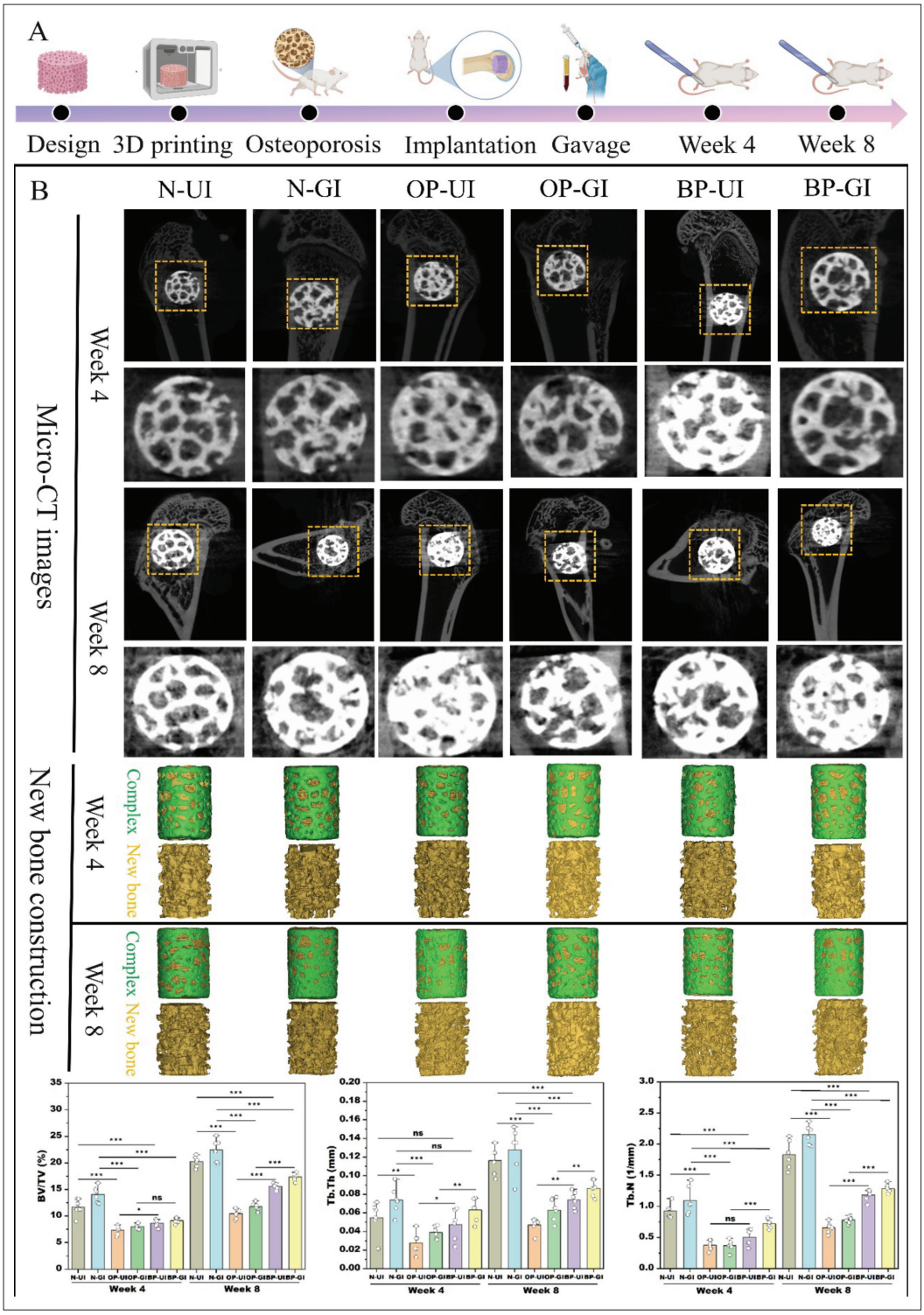

Figure 8. *In vivo* osseointegration analysis. (A) Schematic illustration of scaffold implantation for osseointegration. (B) Quantification of new bone from micro-CT images of bone–scaffold complexes, including reconstruction and measurement of BV/TV, Tb.Th, and Tb.N of new bone (n = 6). Data are expressed as the mean ± standard deviation. *p < 0.05, **p < 0.01, ***p < 0.001, and ****p < 0.0001 indicate statistical significance. Abbreviations: ns: no statistical significance; 3D: three-dimensional; BP: bio-psoralen; BV/TV: bone volume fraction; CT: computed tomography; GI: graded irregular; N: normal; OP: osteoporosis; Tb.N: trabecular number; Tb.Th: trabecular thickness; UI: uniform irregular.

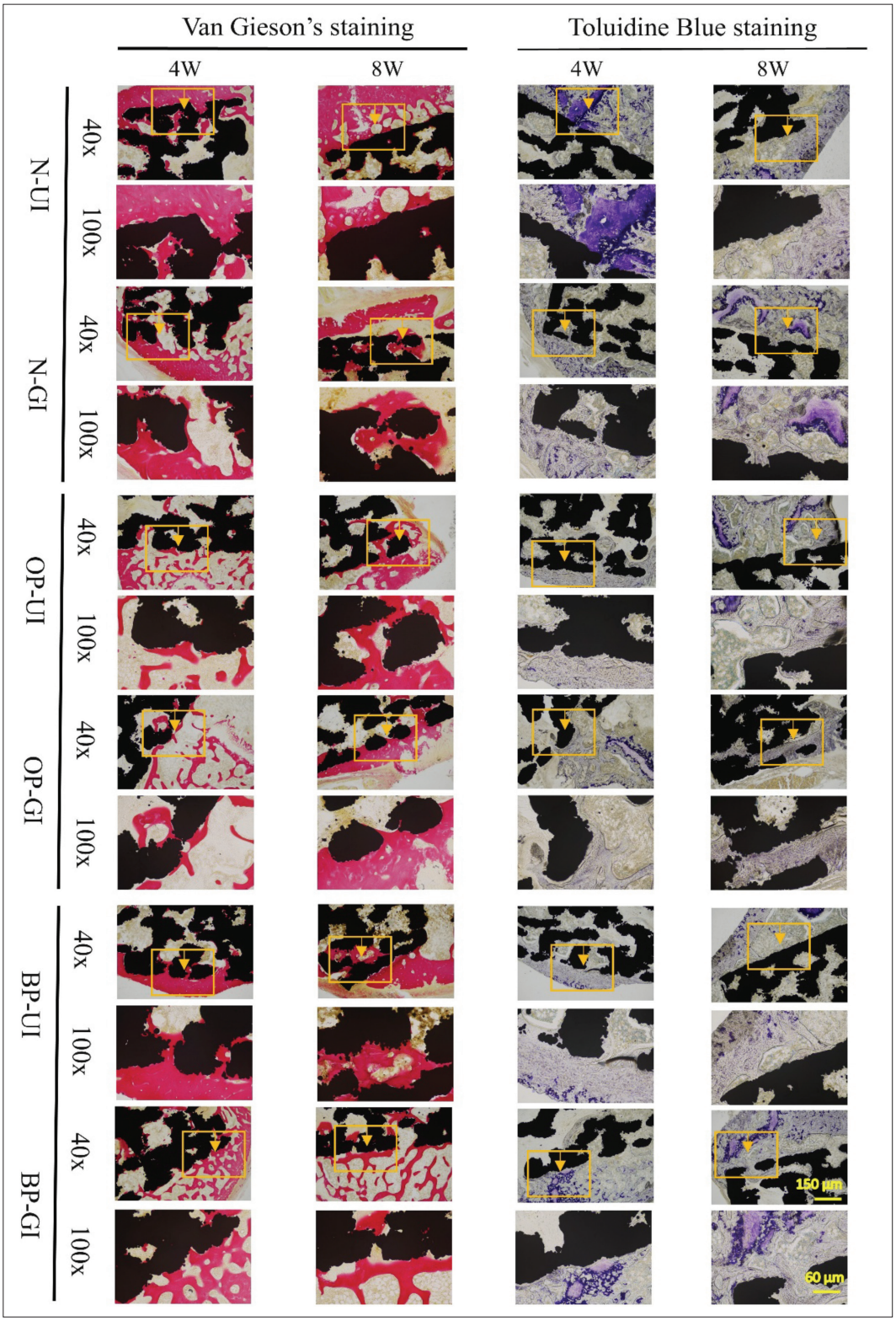

Figure 9. Histological analysis of new bone using Van Gieson's and Toluidine Blue staining (scale bar: 150 μm, magnification: 40×; scale bar: 60 μm, magnification: 100×). Abbreviations: BP: bio-psoralen; GI: graded irregular; N: normal; OP: osteoporosis; UI: uniform irregular.

groups was higher than in OP-scaffold groups, and in GI groups was higher than in UI groups.

3.4. Micro-computed tomography reconstruction and quantitative analysis

All implants were confirmed to be infection-free and stable before harvest. Osseointegration was assessed in Sprague–Dawley rats (Figure 8A). Micro-CT two-dimensional reconstructions visualized new bone ingrowth at weeks 4 and 8. Quantitative 3D analysis showed significantly higher BV/TV (%), Tb.Th, and Tb.N in BP-scaffolds vs. OP-scaffolds, and in GI vs. UI scaffolds (Figure 8B).

3.5. Histological analysis

Histological analysis showed new bone formation progressing from scaffold edges toward the inner pores, as confirmed by both VG and Toluidine Blue staining (Figure 9). Toluidine Blue specifically highlighted new osteoid and mineralized bone in deeper regions. These spatial patterns corresponded to the micro-CT reconstructions, validating osseointegration.

4. Discussion

This study explored the role of psoralen in promoting osseointegration of titanium alloy scaffolds in an osteoporotic environment by regulating macrophage polarization via oral administration. The findings revealed that psoralen promotes macrophage polarization toward the M2 anti-inflammatory phenotype, thereby inducing the osteogenic differentiation of mesenchymal stem cells *in vitro*. Compared with psoralen-coated tissue-engineering scaffolds, oral administration enables long-term delivery, maintains a more stable systemic drug concentration, and achieves long-term efficacy.

Due to the excellent biocompatibility and low cytotoxicity of titanium alloy,[14] it exerts minimal influence on scaffold-conditioned media under different conditions. Conversely, the culture media under varying conditions do not cause significant erosion or structural changes to the titanium alloy surface.[15,16] Therefore, the effects of osteoporotic serum and psoralen-containing serum on the viability and osteogenic differentiation of mesenchymal stem cells cultured within 3D scaffolds can be accurately assessed.

Based on the findings, the stable pH profiles across all groups (Figure 3B) and preserved scaffold integrity after 4 weeks of immersion (Figure 4) confirmed material stability.[17] Critically, BP-scaffolds significantly enhanced BMSC viability compared with scaffolds exposed to osteoporotic serum. Live/dead staining revealed progressive cell death in OP groups at days 4 and 7, whereas BP groups maintained viability comparable to normal scaffolds (Figure 5). Furthermore, CCK-8 results indicated that treatment with psoralen-containing serum partially rescued the impaired proliferation capacity of BMSCs under osteoporotic conditions,[18] exhibiting intermediate activity between normal and OP groups (Figure 3C).

Evidence suggests that in osteoporosis, serum levels of Th17 cytokines (e.g., IL-17) are elevated, whereas regulatory T cell (Treg) cytokines (e.g., IL-10) are reduced, leading to a pro-inflammatory state.[19–21] However, psoralen-containing serum from treated individuals shows a significant decrease in Th17 secretion and an increase in Treg secretion.[22] This is accompanied by downregulation of the transcription factor retinoic acid-related orphan receptor γt and upregulation of forkhead box P3, thereby correcting the immune imbalance.[23]

Osteoporosis deteriorates the bone microenvironment, leading to the release of inflammatory factors and consequently increasing serum cytokine levels. Intervention with psoralen can improve the bone microenvironment, reducing the release of inflammatory factors.[24,25] Specifically, psoralen reduces pro-inflammatory Th1/M1 cytokines (e.g., TNF-α, IL-1β, IFN-γ, IL-2) and increases anti-inflammatory/M2 cytokines (e.g., IL-4, IL-6, IL-10). The reduction in TNF-α and IL-1β removes a major stimulus for osteoclast formation and activity, whereas the increase in IL-4 and IL-10 directly inhibits osteoclastogenesis and supports bone formation.[2,26]

Flow cytometry analysis revealed a notable polarization shift: BP-scaffolds significantly increased the M2/M1 macrophage ratio compared with OP-scaffolds (Figure 6A), indicating effective immunomodulation.[27,28] This finding was further supported by cytokine profiles, which showed that BP-scaffolds suppressed pro-inflammatory mediators (e.g., TNF-α, IL-1β, IL-6; Figure 6B–D) while promoting anti-inflammatory factors (e.g., IL-1Ra, IL-10, arginase; Figure 6E–G). Importantly, the cytokine levels in the BP group remained below those of normal controls, suggesting only partial reversal of OP-associated inflammation.

The impact of macrophage polarization on osteogenic differentiation is central to bone immune regulation.[29] M1 macrophages primarily inhibit osteogenic differentiation and disrupt the osteogenic microenvironment through the secretion of pro-inflammatory factors. In contrast, M2 macrophages strongly promote osteogenic differentiation both directly and indirectly by releasing anti-inflammatory, growth-promoting, and angiogenic factors.[30] BP-scaffolds exhibited significantly superior performance over OP-scaffolds in terms of ALP activity and mineralized nodule

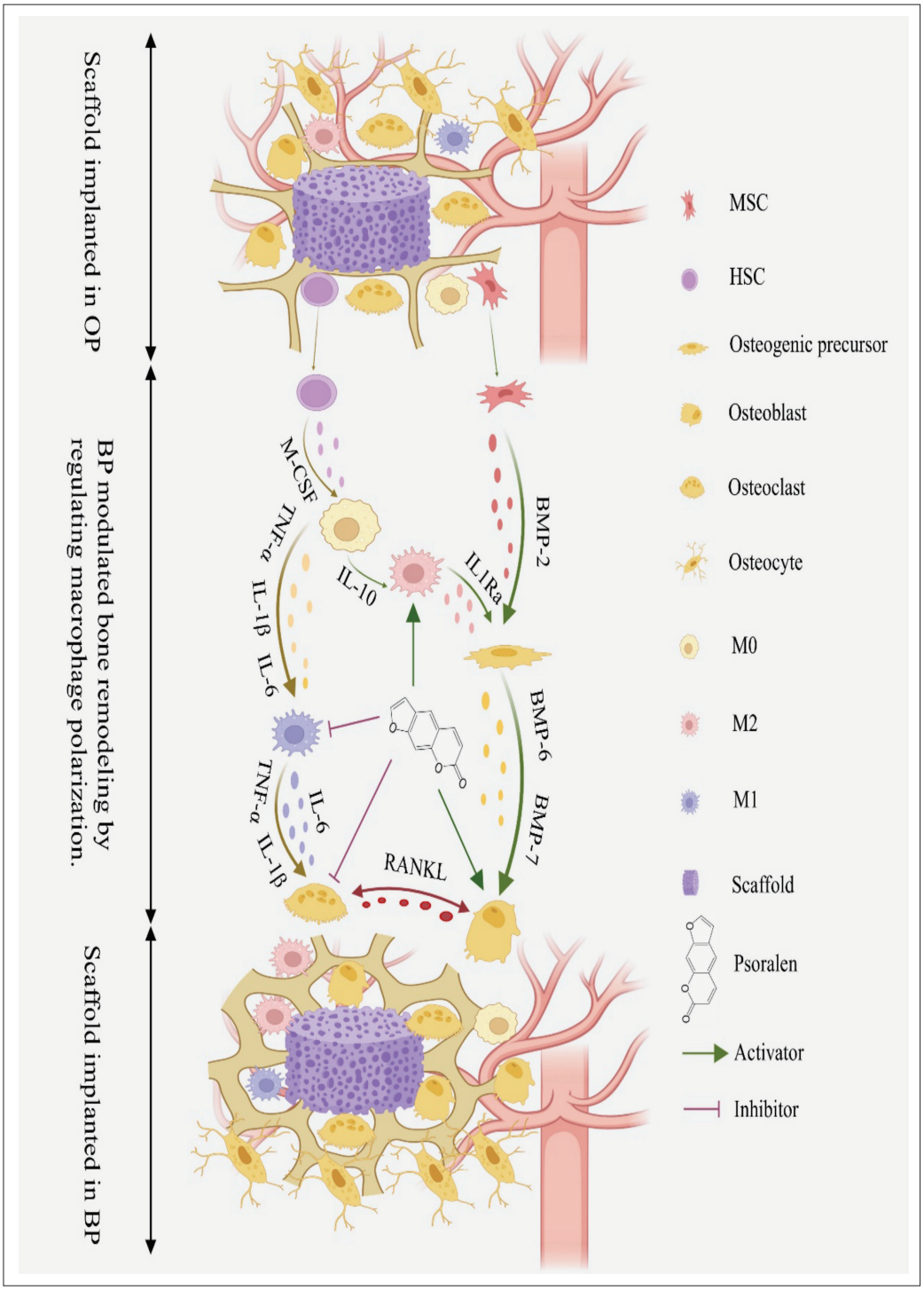

Figure 10. Mechanism of macrophage polarization-mediated bone remodeling around osteoporotic implants regulated by BP. Abbreviations: BP, biopsoralen; HSC, hematopoietic stem cell; MSC, mesenchymal stem cell; OP, osteoporosis.

formation (Figure 7A–C), along with enhanced expression of osteogenic genes (e.g., *Alp*, *Opn*, *Ocn*, *Col1*, *Runx2*; Figure 7D–M). The coordinated upregulation of early markers (e.g., *Runx2*, *Alp*) alongside late markers (*Ocn* and mineralization) indicates that BP-scaffolds effectively support the complete cascade of osteogenic differentiation (Figure 10).[31,32] Additionally, the GI structure showed significant advantages over the UI structure in regulating the polarization of M2 macrophages, enhancing *in vitro* osteogenic differentiation, and promoting *in vivo* bone integration.

However, several limitations remain in this study. First, although Sprague-Dawley rats and their derived mesenchymal stem cells serve as a valid model for osteoporosis research, they may differ from human postmenopausal osteoporosis in bone metabolic characteristics, potentially limiting clinical translation.[33] Second, with the advancement of organoid and organ-on-a-chip technologies, future studies utilizing 3D culture systems may provide greater potential for dynamically investigating the effects of biomaterials on osteoporosis and psoralen interventions.[34–36] Third, the molecular pathways governing psoralen-mediated macrophage polarization (e.g., NF-κB/STAT signaling) remain uncharacterized, requiring validation through knockout studies.[37] Fourth, the 8-week experimental period is insufficient to evaluate the long-term impact of psoralen on bone remodeling in the context of chronic osteoporosis.[38] Finally, this study employed oral administration. Individual differences in serum drug concentrations may affect therapeutic outcomes. Recently, drug-coated scaffolds with local delivery have been proposed as an alternative, but ensuring stability and sustained release of the drug coating remains a challenge.[39]

5. Conclusion

The findings demonstrate that psoralen may promote osteogenic differentiation and scaffold osseointegration in osteoporotic bone by regulating macrophage polarization toward the M2 phenotype *in vitro*. Furthermore, the gradient scaffold structure may synergize with psoralen to enhance M2 macrophage-mediated osteogenic effects *in vitro*. This study provides novel intervention strategies for osteoporotic bone repair and the osseointegration of osteoporotic prostheses, and offers a new perspective for mechanistic investigations of psoralen treatment of osteoporosis.

Acknowledgments

We would like to thank the professors of the Pharmacological Medical Research Center at Zhongshan Hospital of Traditional Chinese Medicine, affiliated with Guangzhou University of Chinese Medicine, for their guidance and for providing experimental facilities and equipment for this study.

Funding

This work was supported by the Traditional Chinese Medicine Inheritance Innovation Development Research Project of Zhongshan City (No. 2024B3019) and China Postdoctoral Science Foundation (No. 2024M750668). The funders had no role in the design of the study, the collection, analysis, and interpretation of the data, or in writing the manuscript.

Conflict of interest

The authors declare that they have no competing interests.

Author contributions

Conceptualization: Jijie Peng
Data curation: Jingyang Chen
Formal analysis: Di Che
Funding acquisition: Yuzhu Wang
Investigation: Siyan Chen
Methodology: Jian Ji
Project administration: Junzhe Wu
Resources: Yuzhu Wang
Software: Yilong Wu
Supervision: Yuzhu Wang
Validation: Yue Meng
Visualization: Xingmao Zhou
Writing–original draft preparation: Jian Ji
Writing–review and editing: Yufeng He
All authors have read and agreed to the published version of the manuscript.

Ethics approval and consent to participate

The animal research protocol was approved by the Ethics Committee of Zhongshan Hospital of Traditional Chinese Medicine Affiliated to Guangzhou University of Chinese Medicine (No. AEWC-2023008). The animals were obtained from Guangdong Medical Animal Laboratory Center for medical research purposes (approval no. SCXK 2022-0002).

Consent for publication

Not applicable.

Availability of data

The data are available from the corresponding authors upon reasonable request.

References

1. Johnston CB, Dagar M. Osteoporosis in older adults. *Med Clin North Am*. 2020;104(5):873-884. doi: 10.1016/j.mcna.2020.06.004
2. Ren Y, Song X, Tan L, *et al*. A review of the pharmacological properties of psoralen. *Front Pharmacol*. 2020;11:571535. doi: 10.3389/fphar.2020.571535
3. An J, Yang H, Zhang Q, *et al*. Natural products for treatment of osteoporosis: the effects and mechanisms on promoting osteoblast-mediated bone formation. *Life Sci*. 2016;147:46-58. doi: 10.1016/j.lfs.2016.01.024
4. Li F, Li Q, Huang X, *et al*. Psoralen stimulates osteoblast proliferation through the activation of nuclear factor-κB-mitogen-activated protein kinase signaling. *Exp Ther Med*. 2017;14(3):2385-2391. doi: 10.3892/etm.2017.4771
5. Li JP, Xie BP, Zhang WJ, *et al*. Psoralen inhibits RAW264.7 differentiation into osteoclasts and bone resorption by regulating CD4+T cell differentiation. *Zhongguo Zhong Yao Za Zhi*. 2018;43(6):1228-1234. Chinese. doi: 10.19540/j.cnki.cjcmm.20180104.017
6. Isa AI, Fouotsa H, Mohammed OA, *et al*. Psoralen isolated from the roots of *Dorstenia psilurus* Welw. Modulate Th1/Th2 cytokines and inflammatory enzymes in LPS-stimulated RAW 264.7 macrophages. *Mediators Inflamm*. 2024;2024:8233689. doi: 10.1155/2024/8233689
7. Guo Y, Xu S, Pan X, *et al*. Psoralen protects neurons and alleviates neuroinflammation by regulating microglial M1/M2 polarization via inhibition of the Fyn-PKCδ pathway. *Int Immunopharmacol*. 2024;137:112493. doi: 10.1016/j.intimp.2024.112493
8. Luo L, Zheng W, Li J, *et al*. 3D-printed titanium trabecular scaffolds with sustained release of hypoxia-induced exosomes for dual-mimetic bone regeneration. *Adv Sci (Weinheim)*. 2025;12(23):e2500599. doi: 10.1002/advs.202500599
9. Pirogova Y, Tashkinov M, Vindokurov I, *et al*. Design of lattice structures for trabecular-bone scaffolds: comparative analysis of morphology and compressive mechanical behaviour. *Biomech Model Mechanobiol*. 2025;24(5):1535-1564. doi: 10.1007/s10237-025-01980-5
10. Walczak M, Okuniewski W, Nowak WJ, Chocyk D, Pasierbiewicz K. Corrosion behavior of shot peened Ti6Al4V alloy fabricated by conventional and additive manufacturing. *Materials (Basel)*. 2025;18(10):2274. doi: 10.3390/ma18102274
11. Xu M, Lin Y, Lin Z, Cheng H. Elastic and fatigue properties of additively manufactured and milled Ti-6Al-4V removable partial denture clasps. *J Prosthet Dent*. 2025;133(1):230.e1-230.e8. doi: 10.1016/j.prosdent.2024.09.017
12. Wang Y, Ma C, Wu Y, Gao D, Meng Y, Wang H. Comprehensive evaluation of biomechanical and biological properties of the porous irregular scaffolds based on voronoi-tessellation. *J Bionic Eng*. 2025;22:322-340. doi: 10.1007/s42235-024-00630-3
13. Wang Y, Wu Z, Li C, *et al*. Effect of bisphosphonate on bone microstructure, mechanical strength in osteoporotic rats by ovariectomy. *BMC Musculoskelet Disord*. 2024;25(1):725. doi: 10.1186/s12891-024-07846-8
14. Sartori M, Bregoli C, Carniato M, *et al*. Biological characterization of Ti6Al4V additively manufactured surfaces: comparison between ultrashort laser texturing and conventional post-processing. *Adv Healthc Mater*. 2025;14(4):e2402873. doi: 10.1002/adhm.202402873
15. Yan K, Ngadiman NHA, Saman MZM, Mustafa NS. Advancements in selective laser melting (SLM) of titanium alloy scaffolds for bone tissue engineering. *Biofabrication*. 2025;17(2):022016. doi: 10.1088/1758-5090/adc6c0
16. Habijan T, Haberland C, Meier H, *et al*. The biocompatibility of dense and porous nickel-titanium produced by selective laser melting. *Mater Sci Eng C Mater Biol Appl*. 2013;33(1):419-426. doi: 10.1016/j.msec.2012.09.008
17. Sevcikova J, Pavkova Goldbergova M. Biocompatibility of NiTi alloys in the cell behaviour. *Biometals*. 2017;30(2):163-169. doi: 10.1007/s10534-017-0002-5
18. Si Y, Dong S, Li M, *et al*. Curcumin-encapsulated exosomes in bisphosphonate-modified hydrogel microspheres promote bone repair through macrophage polarization and DNA damage mitigation. *Mater Today. Bio*. 2025;32:101874. doi: 10.1016/j.mtbio.2025.101874
19. Peng P, Wong P, Lv Z, *et al*. Tectorigenin ameliorates glucocorticoid-induced osteoporosis by inhibiting the NF-κB signal pathway and modulating Treg-Th17 cell balance. *J Cell Mol Med*. 2025;29(13):e70705. doi: 10.1111/jcmm.70705
20. Shen X, Zhang Q, Ding J, *et al*. Licochalcone D inhibits osteoclast differentiation and postmenopausal osteoporosis by inactivating the NF-κB signaling pathway. *J Orthop Surg Res*. 2025;20(1):713. doi: 10.1186/s13018-025-06132-0
21. Ma Z, Liu Y, Shen W, *et al*. Osteoporosis in postmenopausal women is associated with disturbances in gut microbiota and migration of peripheral immune cells. *BMC musculoskeletal disorders*, 2024;25(1):791. doi: 10.1186/s12891-024-07904-1

22. Talaat RM, Sidek A, Mosalem A, Kholief A. Effect of bisphosphonates treatment on cytokine imbalance between TH17 and Treg in osteoporosis. *Inflammopharmacology.* 2015;23(2–3):119-125.
doi: 10.1007/s10787-015-0233-4

23. Chen Z, Lin F, Gao Y, *et al.* FOXP3 and RORγt: transcriptional regulation of Treg and Th17. *Int Immunopharmacol.* 2011;11(5):536-542.
doi: 10.1016/j.intimp.2010.11.008

24. Weng Z, Ye J, Cai C, *et al.* Inflammatory microenvironment regulation and osteogenesis promotion by bone-targeting calcium and magnesium repletion nanoplatform for osteoporosis therapy. *J Nanobiotechnol.* 2024:22(1):314.
doi: 10.1186/s12951-024-02581-7

25. Xu W, Zhang Y, Huang X, *et al.* Alendronate carbon dots targeting bone immune microenvironment for the treatment of osteoporosis. *Chem Eng J*. 2024;494:152209.
doi: 10.1016/j.cej.2024.152209

26. Maruthamuthu V, Henry LJK, Ramar MK, Kandasamy R. Myxopyrum serratulum ameliorates airway inflammation in LPS-stimulated RAW 264.7 macrophages and OVA-induced murine model of allergic asthma. *J Ethnopharmacol.* 2020;255:112369.
doi: 10.1016/j.jep.2019.112369

27. Wu S, Ma J, Liu J, *et al.* Immunomodulation of telmisartan-loaded PCL/PVP scaffolds on macrophages promotes endogenous bone regeneration. *ACS Appl Mater Interfaces.* 2022;14(14):15942-15955.
doi: 10.1021/acsami.1c24748

28. Abedi N, Sadeghian A, Kouhi M, *et al.* Immunomodulation in bone tissue engineering: recent advancements in scaffold design and biological modifications for enhanced regeneration. *ACS Biomater Sci Eng.* 2025; 11(3): 1269-1290.
doi: 10.1021/acsbiomaterials.4c01613

29. Ji X, Yuan X, Ma L, *et al.* Mesenchymal stem cell-loaded thermosensitive hydroxypropyl chitin hydrogel combined with a three-dimensional-printed poly(ε-caprolactone) / nano-hydroxyapatite scaffold to repair bone defects via osteogenesis, angiogenesis and immunomodulation. *Theranostics.* 2020;10(2):725-740.
doi: 10.7150/thno.39167

30. Zhang F, Lv M, Wang S, *et al.* Ultrasound-triggered biomimetic ultrashort peptide nanofiber hydrogels promote bone regeneration by modulating macrophage and the osteogenic immune microenvironment. *Bioact Mater.* 2023;31:231-246.
doi: 10.1016/j.bioactmat.2023.08.008

31. Song Q, Zhang Y, Hu H, *et al.* Multifunctional hydrogel with synergistic reactive oxygen species scavenging and macrophage polarization-induced osteo-immunomodulation for enhanced bone regeneration. *ACS Appl Mater Interfaces.* 2025;17(27):38985-39001.
doi: 10.1021/acsami.5c08737

32. Wu M, Liu H, Li D, *et al.* Smart-responsive multifunctional therapeutic system for improved regenerative microenvironment and accelerated bone regeneration via mild photothermal therapy. *Adv Sci (Weinh).* 2024;11(2):e2304641.
doi: 10.1002/advs.202304641

33. Xu L, Zhu J, Rong L, *et al.* Osteoblast-specific down-regulation of NLRP3 inflammasome by aptamer-functionalized liposome nanoparticles improves bone quality in postmenopausal osteoporosis rats. *Theranostics.* 2024;14(10):3945-3962.
doi: 10.7150/thno.95423

34. Hu Y, Zhang H, Wang S, *et al.* Bone/cartilage organoid on-chip: construction strategy and application. *Bioact Mater.* 2023;25:29-41.
doi: 10.1016/j.bioactmat.2023.01.016

35. Kong Y, Yang Y, Hou Y, Wang Y, Li W, Song Y. Advance in the application of organoids in bone diseases. *Front Cell Dev Biol.* 2024;12:1459891.
doi: 10.3389/fcell.2024.1459891

36. Bai L, Zhou D, Li G, Liu J, Chen X, Su J. Engineering bone/cartilage organoids: strategy, progress, and application. *Bone Res.* 2024;12(1):66.
doi: 10.1038/s41413-024-00376-y

37. Rogers TL, Holen I. Tumour macrophages as potential targets of bisphosphonates. *J Transl Med.* 2011;9:177.
doi: 10.1186/1479-5876-9-177

38. Brown JP. Long-term treatment of postmenopausal osteoporosis. *Endocrinol Metab (Seoul)*. 2021;36(3):544-552.
doi: 10.3803/EnM.2021.301

39. Su N, Villicana C, Zhang C, *et al.* Aspirin synergizes with mineral particle-coated macroporous scaffolds for bone regeneration through immunomodulation. *Theranostics.* 2023;13(13):4512-4525.
doi: 10.7150/thno.85946